Theory of momentum-resolved phonon spectroscopy in the electron microscope

R.J. Nicholls,[1,*] F.S. Hage,[2] D.G. McCulloch,[3] Q.M. Ramasse,[2,4] K. Refson,[5,6] and J.R. Yates[1]

[1] *Department of Materials, University of Oxford, Parks Road, Oxford, OX1 3PH, United Kingdom*

[2] *SuperSTEM Laboratory, SciTech Daresbury Campus, Keckwick Lane, Warrington, WA4 4AD, United Kingdom*

[3] *Physics, School of Sciences, RMIT University, Melbourne, VIC 3001, Australia*

[4] *School of Physics and School of Chemical and Process Engineering, University of Leeds, Leeds LS2 9JT, United Kingdom*

[5] *Department of Physics, Royal Holloway, University of London, Egham TW20 0EX, United Kingdom*

[6] *ISIS Spallation Neutron Source, RAL, Chilton, Didcot OX11 0QX, United Kingdom*

We provide a theoretical framework for the prediction and interpretation of momentum dependent phonon spectra due to coherent inelastic scattering of electrons. We complete the approach with first principles lattice dynamics using periodic density functional theory and compare to recent electron energy loss measurements on cubic and hexagonal boron nitride performed within a scanning transmission electron microscope (STEM). The combination of theory and experiment provides the ability to interpret momentum dependent phonon spectra obtained at nanometer spatial resolution in the electron microscope.

The quantitative description of the thermal physics of solid materials in terms of quantized lattice vibrations, phonons, is one of the major achievements of condensed-matter physics in the 20th century. Lattice dynamics is central to the theories of phenomena including structural phase transitions, superconductivity, thermal expansion, thermal conductivity, stability of polymorphs and much more. Laboratory techniques to measure phonon spectra using light including infra-red and Raman spectroscopy are powerful and widely deployed across laboratories, but the energy-momentum relation of the photon probe restricts the interaction with phonons to involve essentially zero momentum transfer. Consequently only a subset of phonon modes at the long-wavelength limit may be measured using optical probes.

Inelastic neutron scattering (INS), pioneered by Bertram Brockhouse [1], was the major development which enabled the full measurement of phonon spectra at all phonon wavevectors - the first momentum-resolved spectroscopy. This was followed by inelastic X-Ray scattering (IXS) [2, 3, and citations therein]. Such techniques have been the mainstay of phonon spectroscopy in crystalline solids for half a century. However their application is limited by the scarcity and expense of INS and IXS spectrometers, which must be based at reactor, accelerator or synchrotron sources. The requirement to grow single crystal specimens also limits their widespread use, particularly in the case of neutrons where crystal sizes of 20-1000mm^3 are needed. The spatial resolution of INS is larger than 1cm, and while X-Ray beams can focus to 25μm, counting rates and experimental timescales mostly preclude spatially-resolved studies.

Electrons have been used since the 1960s in a reflection geometry to measure the average surface response of a material [4, 5]. Recent advances in source monochromation mean that it is now possible to measure phonon spectra in a transmission electron microscope using electron energy-loss spectroscopy (EELS) with a resolution of 15meV or better [6]. This adds a complementary technique to the methods above, with the additional advantages of nanometer spatial resolution [6, 7] of the phonon spectrum, alongside atomically resolved chemical and structural analysis, all within the same instrument.

The theory of INS from phonons was developed in a very general formalism by Leon van Hove [8], and can be adapted to any radiative probe for which the interaction Hamiltonian is known. In this paper we present its extension to coherent inelastic scattering of electrons from phonons and apply it to the case of momentum-resolved EELS experiments performed in a scanning transmission electron microscope (STEM). This formalism enables the prediction of scattering cross section as a function of momentum and energy transfer and makes possible a quantitative comparison with EELS experiments. It reveals the fundamental physics shared between inelastic scattering of electrons, neutrons and photons, and attempts to unify the theories of EELS, INS and IXS. In contrast, previous work has looked at specific cases [9–11], been used to interpret the $q = 0$ modes in a nanocube [12, 13], has looked at spatial the effects of beam geometry [14] or dealt with the dipole ($q \approx 0$) scattering regime [15, 16]. We apply this general method to predict the phonon contribution to the EEL spectrum of two polymorphs of boron nitride and make a direct comparison to their recently-measured momentum-resolved spectra [17].

As the energy transfer that occurs in the scattering process is small compared to that of the scattered particle, the double differential cross section is given by the Born approximation as [18]

$$\frac{d^2\sigma}{d\Omega dk_1} = \frac{1}{N}\frac{N_0 V \sum_{n_0,n_1} P_{n_0} k_1^2 |\langle n_0, \mathbf{k}_0 | H_{inter} | n_1, \mathbf{k}_1 \rangle|^2 \delta(E_{n_0} + E_0 - E_{n_1} - E_1)}{(2\pi)^2 \hbar (j_0)_z} \tag{1}$$

where n_0 and n_1 are the initial and final states of the material with energies E_{n_0} and E_{n_1} respectively, $\mathbf{k}_0$ and $\mathbf{k}_1$ are the initial and final states of the scattered particle with energies E_0 and E_1 respectively, H_{inter} is the Hamiltonian for the interaction of the particle with the material, $(j_0)_z$ is the current density of the beam of particles in the z-direction, P_{n_0} is the probability of finding the material in state n_0 before scattering, N is the number of scatterers in the material, N_0 is the number of electrons in state k_0 and V is the volume of the unit cell. The scattered particle could be photons, neutrons or fast electrons. For the different particles, a different form for the interaction Hamiltonian, and a different expression for the current density, is used. The fast electron will interact with both the electrons and nuclei in the sample and the interaction Hamiltonian can be written as

$$H_{inter}(\mathbf{r}) = \frac{-e}{4\pi\epsilon_0}\int \frac{\rho_{tot}(\mathbf{r}')}{|\mathbf{r}-\mathbf{r}'|} d\mathbf{r}' \tag{2}$$

where $\mathbf{r}$ is the fast electron position, $\mathbf{r}'$ is the material coordinate, e is the magnitude of charge of an electron and ρ_{tot} is the total charge density containing both the nuclear and electronic contributions. Here we have assumed a material with no spin density in the ground state. Retardation effects have also been neglected. Before and after the scattering event, the fast electron and material do not interact, so we can write $|n_0, \mathbf{k}_0\rangle = |n_0\rangle|\mathbf{k}_0\rangle$ and $|n_1, \mathbf{k}_1\rangle = |n_1\rangle|\mathbf{k}_1\rangle$. By including the full interaction Hamiltonian in equation 1, defining the momentum transfer from the fast electron to the sample as $\mathbf{q} = \mathbf{k}_0 - \mathbf{k}_1$, approximating the fast electron as a plane wave, writing the energy transfer as $\hbar\omega$ and writing $(j_0)_z$ as $\frac{N_0}{V}\frac{\hbar k_0}{m}$, equation 1 becomes

$$\frac{d^2\sigma}{d\Omega dE_1} = \frac{m^2e^2}{\hbar^4 q^4 \epsilon_0^2 4\pi^2}\frac{k_1}{k_0}\frac{1}{N}\sum_{n_0,n_1} P_{n_0} |\langle n_0| \int d\mathbf{r}' e^{-2\pi i \mathbf{q}.\mathbf{r}'} \rho_{tot}(\mathbf{r}') |n_1\rangle|^2 \delta(E_{n_0} - E_{n_1} + \hbar\omega) \tag{3}$$

Following Van Hove [8], the double differential cross section can be written in terms of a scattering function, $S(q,\omega)$

$$\frac{d^2\sigma}{d\Omega dE_1} = \frac{m^2e^2}{\hbar^4 q^4 \epsilon_0^2 4\pi^2}\frac{k_1}{k_0}\frac{1}{N} S(q,\omega) \tag{4}$$

To determine $S(q,\omega)$ we follow the general approach of Sinha [19] and Burkel [20] who considered X-Ray scattering from phonon vibrations. We first assume that the total charge density can be expressed as a sum of atomic charge densities. This is clearly a major simplification, and we return to this approximation later. We also assume harmonic lattice dynamics in a crystal and can hence express the lattice vibrations expressed as phonon eigenvectors. By neglecting processes involving multiple phonons, we obtain an expression for $S(q,\omega)$ for the creation of phonons by a fast electron:

$$S(q,\omega) = \left| \sum_i F(\mathbf{q}, Z_i) e^{-W_i} [\mathbf{q}.\mathbf{e}_i(\mathbf{q}_0, j)] M_i^{-1/2} e^{i\mathbf{q}.\mathbf{r}_i} \right|^2 \frac{1}{\omega_{\mathbf{q}_0 j}} \delta(\omega - \omega_{\mathbf{q}_0 j}) \tag{5}$$

where there are i atoms per unit cell at positions $\mathbf{r}_i$, M_i and Z_i are the mass and atomic number of atom i, $\mathbf{e}_i(\mathbf{q}_0, j)$ is the phonon eigenvector with wavevector $\mathbf{q}_0$ (defined in the first Brillouin Zone) and polarisation branch j at atom i and e^{-2W_i} is the Debye-Waller factor. $F(\mathbf{q}, Z_i)$ is given by

$$F(\mathbf{q}, Z_i) = f_{atom,i}(\mathbf{q}) + Z_i e \tag{6}$$

where $f_{atom,i}(\mathbf{q})$ is the atomic form factor.

The scattering factor obtained for the interaction of electrons with phonons is very similar to those obtained for X-Rays and neutrons [11], highlighting the complementary nature of the techniques. As is the case with X-Rays and neutrons, equation 5 contains a term $\mathbf{q}.\mathbf{e}_i(\mathbf{q}_0, j)$, the dot product between the momentum transfer and the phonon eigenvector. This means that

only modes with motion in the same direction as the momentum transfer will appear in the spectra. Equation 5 has a q^2 dependence which, when combined with the q^{-4} term in equation 4, means that in the case of electrons, the double differential cross section has a q^{-2} dependence and diverges as $q \to 0$. The $q = 0$ case corresponds to zero scattering angle; in a STEM experiment data is collected over a range of angles and so the divergence is washed out. This q^{-2} dependence results from the Coulombic form of the interaction between the fast electron and the charge density in the material. This is not the case for neutrons and X-Rays where the different interaction Hamiltonians result in a q^2 dependence. From a practical point of view, this means that experimental data using these techniques is rarely collected from the first Brillouin Zone as large values of q will give a greater signal. When using electrons, the signal will be strongest within the first Brillouin Zone.

The scattering function formalism developed above enables us to go beyond simply comparing momentum-dependent EEL spectra to phonon bandstructures and understanding of the relative contributions of the different modes to the spectra. It has been developed to understand scattering in which there is finite momentum transfer, a regime known as the localised vibrational scattering regime [7]; a correct treatment of the $q = 0$ term would also include dipole scattering [7, 15, 16].

Momentum resolved phonon EEL spectra from both cubic and hexagonal BN are shown in Figure 1. (The experiments were carried out with a beam energy of $60keV$ to reduce the beam damage to the sample. The experimental spectra have been background subtracted [11] and the intensity of the experimental spectrum for each q vector has been normalised. The experiments are described in [11] with further details of the experimental method given in [17, 21].) These spectra can be understood using the scattering factor obtained above for the interaction of a fast electron with the vibrational modes of the material. In order to obtain the phonon eigenvectors, we use density functional perturbation theory as implemented within the CASTEP code [22, 23]. Details of the computational parameters are given in [11]. The effects of charge transfer are significant in BN polymorphs, and as an initial approach to incorporating these effects we replace $F(\mathbf{q}, Z_i)$ in Eq. 6 with

$$F(\mathbf{q}, Z_i) = \frac{f_{atom,i}(\mathbf{q})(Z_i - Z_i^*)}{Z_i} + Z_i e \qquad (7)$$

where Z_i^* is the Mulliken charge computed for atom i. Details of the effect of this approximation on the simulated EEL spectra are given in [11].

The quantity that has been calculated for comparison with experiment is

$$\mathcal{J} = \frac{1}{q^4}\Big|\sum_i \Big(\frac{f_{atom,i}(\mathbf{q})(Z_i - Z_i^*)}{Z_i e} + Z_i\Big) e^{-W_i} [\mathbf{q}.\mathbf{e}(\mathbf{q}_0, j)] M_i^{-1/2} e^{i\mathbf{q}.\mathbf{r}_i}\Big|^2 \frac{1}{\omega_{\mathbf{q}_0 j}} \qquad (8)$$

where the phonon eigenvectors and frequencies, Debye-Waller factors and Mulliken charges are computed using DFT, and atomic-form factors are taken from the literature. $\mathcal{J}$ can be thought of as a relative intensity and it tells us which of the different modes contribute towards the spectrum and by how much compared to the other modes. The calculated EEL spectrum is constructed by combining Gaussians centred on each of the phonon energies, scaled by $\mathcal{J}$. For modes which have an eigenvector orthogonal to q, the spectra intensity will be equal to zero and they will not contribute to the spectrum. Simulated spectra for cBN are included in Figure 1a and a further comparison between spectra in the $\Gamma - \mathrm{K}$ direction is included in [11]. For the comparison with experiment, the simulated loss function has been scaled to match the maximum in the experimental data. As the $q = 0$ term is not well defined, a spectrum has been simulated for $q = 0.01$ for comparison with the experimental data. The spectrum seen at $q = 0$ in the experimental data will have a dipole term, which has not been included here, as well as contributions from small values of momentum transfer as a result of the experimental geometry . The q^{-2} dependence of the cross-section means that it is relatively large for very small, but finite, values of q and that it decreases by approximately six orders of magnitude across the Brillouin zone. Figure 2 shows the corresponding part of the phonon dispersion with the colour of the modes corresponding to how much the modes contribute to the spectrum. Due to the large variation in intensity across the Brillouin zone, it has been plotted on a log_{10} scale. As can be seen from the figure, only two of the six possible phonon modes predicted by DFT for cBN contribute to the spectra, one of these is an optical branch and the other an acoustic branch. For the other modes, the atomic motion is perpendicular to $\mathbf{q}$. Four modes contribute in the $\Gamma - \mathrm{K}$ direction [11]. In that case, a lower energy mode dominates at higher values of q and the spectrum appears to shift as $|\mathbf{q}|$ increases.

Experimental and simulated data for the $\Gamma - \mathrm{K}$ direction in hBN are shown in Figure 1b. The corresponding part of the Brillouin zone showing the contribution of the different modes is shown in Figure 2. In this case,

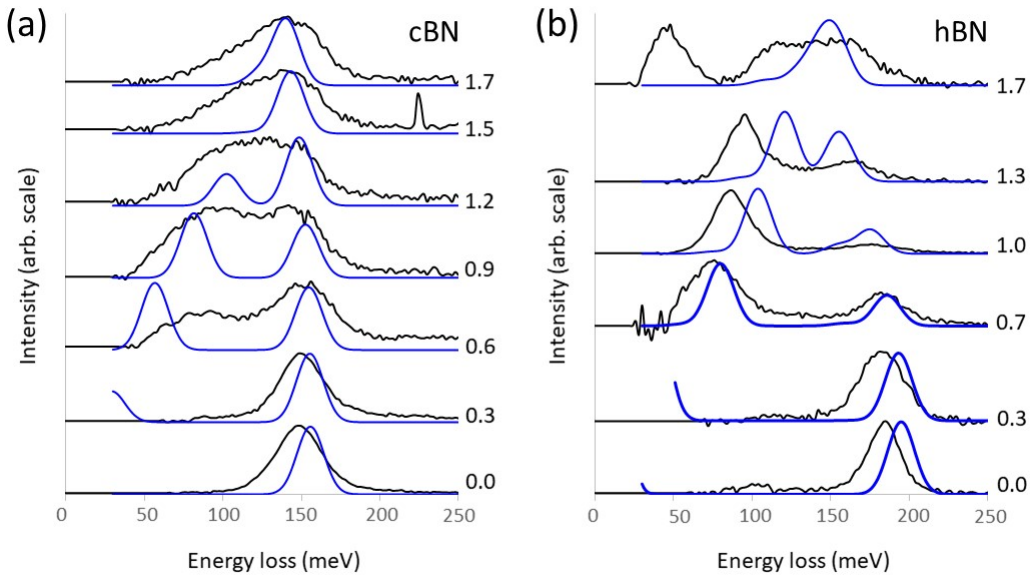

FIG. 1. Experimental (black) and simulated (blue) phonon EEL spectra for (a) the $\Gamma - X$ direction in cubic BN and (b) the $\Gamma - K$ direction in hexagonal BN. Each spectrum is labelled by the corresponding q vector in units of $\AA^{-1}$, given to one decimal place.

four of the twelve DFT-predicted modes contribute to the spectra. Previous work by Serrano *et al.* [24] has shown good agreement between DFT phonon bandstructures and IXS data from hBN. They also showed their phonon bandstructure agreed well with published reflection EELS data from [25]. Our DFT phonon bandstructures are very similar to those reported by Serrano *et al.* [24] but the agreement between our simulated and experimental data for hBN is not as good in the cBN case and this is likely to be due partly to our treatment of the so-called LO-TO splitting. In an infinite crystal, the longitudinal optical (LO) mode is blue-shifted by the interaction between macroscopic electric fields generated by displaced ions as $q \rightarrow 0$ and the ionic charges. In a crystal of finite thickness, joint electromagnetic cavity and phonon modes known as phonon polaritons appear with energies intermediate between the LO and TO values. These modes, display strong dependence when thickness is comparable to the optical wavelength. Our calculations have included the LO-TO splitting expected for an infinite crystal whilst the experimental data was collected from a crystal of a thickness where the phonon polaritons are expected to show significant thickness dependence [16, 17]. Michel and Verberck [26] calculated the phonon dispersion of hBN multilayers. Their work shows this effect will only affect the upper two branches that contribute towards the spectrum. Near the Γ-point the two branches are further apart in the case of an infinite crystal and the difference between a multilayer and 3D crystal decreases as $\mathbf{q} \rightarrow \mathbf{K}$. Theoretically, the uppermost branch dominates near the Γ-point and so the simulations will over-estimate the peak position. For the other values of q, the lower branch dominates and so the simulations will be less affected. This is what we see in Figure 1b.

Another factor contributing to the discrepancy between simulation and experiment is the experimental geometry. The experimental momentum resolution results in data being collected over a small range of q vectors; this is currently not included in our calculations. In addition our calculations include in-plane contributions only whilst the curvature of the Ewald Sphere will mean that the contribution of modes with an out-of-plane q component will increase as q increases. This is seen in our data where, for larger values of q, the match between experiment and theory is less good. The experimental peak positions are close to phonon energies in the dispersion, but not ones that would be expected to contribute towards the spectrum due to the $\mathbf{q}.\mathbf{e}(\mathbf{q}_0, j)$ term. The finite size of the probe may also have an effect on the spectrum with local inhomogeneities, such as defects, resulting in breaking of symmetry making the $\mathbf{q}.\mathbf{e}(\mathbf{q}_0, j)$ term becomes non-zero. Data showing the $\Gamma - M$ direction shows similar trends (see [11]).

The scattering function formalism developed here highlights the fundamental similarities between the scattering of electrons, neutrons and X-Ray, as well as the differences resulting from the Coulombic interaction. In addition to this, the experimental set up used to collect EELS data means that finite momentum and spatial resolution will also possibly need to be considered when interpreting experimental data.

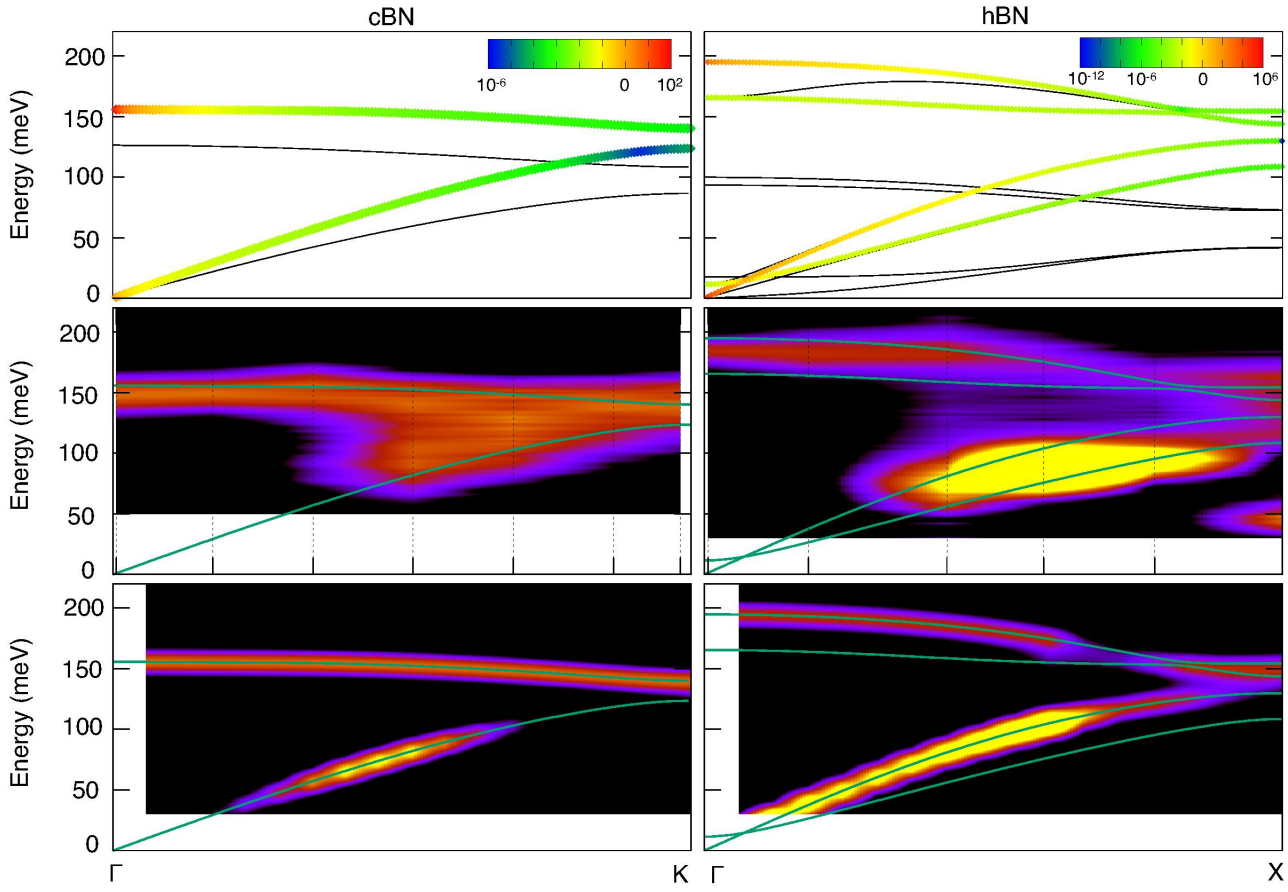

FIG. 2. Comparison of experimental and computed dispersion relations for cBN (left) and hBN (right). Upper panel: Calculated phonon dispersion spectra. The bands are coloured according to their intensity on a log_{10} scale. Inactive bands are shown in black. Middle Panel: Experimental intensity, normalised by the value of the intensity in the upper branch. The momenta at which the data was recorded is shown by dash vertical lines and the plot is generated by interpolating between the datapoints. The computed DFT band structure is shown in green. Lower panel: Computed intensity, normalised by the value of the intensity in the upper branch.

In this paper we have formulated a general expression for the interaction of a fast electron with phonon vibrations inside a STEM. We have applied this approach to understand the differences in momentum resolved EEL spectra from different polymorphs of BN. The simulated spectra match well with the experimental data and allow us to understand which modes are contributing to the spectra. This is a general approach and will allow interpretation of experimental data from a large variety of materials.

SuperSTEM is the UK Engineering and Physical Sciences Research Council (EPSRC) National Research Facility for Advanced Electron Microscopy. RJN gratefully acknowledges financial support from the EPSRC, grant EP/L022907/1. Raw experimental data were generated at the SuperSTEM Laboratory, with *ab initio* modelling carried out at the University of Oxford. Source data is available from the corresponding authors upon reasonable request.

* rebecca.nicholls@materials.ox.ac.uk

[1] B. N. Brockhouse, Reviews of Modern Physics **67**, 735 (1995).
[2] A. Q. R. Baron, "Phonons in crystals using inelastic x-ray scattering," (2009), english version of a paper in Japanese, Journal of The Spectroscopical Society of Japan, 58, 205 (2009), arXiv:0910.5764 English version of a paper in Japanese, Journal of The Spectroscopical Society of Japan, 58, 205 (2009).
[3] M. Krisch and F. Sette, Crystallography Reports **62**, 1 (2017).
[4] F. M. Propst and T. C. Piper, Journal of Vacuum Science and Technology **4**, 53 (1967).
[5] H. Ibach and D. L. Mills, *Electron Energy Loss Spectroscopy and Surface Vibrations* (Academic Press, 1982).
[6] O. L. Krivanek, T. C. Lovejoy, N. Dellby, T. Aoki, R. W. Carpenter, P. Rez, E. Soignard, J. Zhu, P. E. Batson, M. J. Lagos, R. F. Egerton, and P. A. Crozier, Nature **514**, 209 (2014).

[7] C. Dwyer, T. Aoki, P. Rez, S. L. Y. Chang, T. C. Lovejoy, and O. L. Krivanek, Physical Review Letters **117**, 256101 (2016).

[8] L. Van Hove, Physical Review **95**, 249 (1954).

[9] P. Rez, Microsc. Microanal. **20**, 671 (2014).

[10] J. R. M. Saavedra and F. Javier García de Abajo, Physical Review B **92**, 115449 (2015).

[11] See Supplemental Material at [URL] for comments on related treatments and the scattering function formalism for X-rays and neutrons and details of the experiments, first principles calculations, the atomic form factor, the Debye-Waller factor, momentum resolved data for the $\Gamma - K$ direction in cBN and the $\Gamma - M$ direction in hBN and how charge transfer has been included in the simulations.

[12] M. J. Lagos, A. Trügler, U. Hohenester, and P. E. Batson, Nature **543**, 529 (2017).

[13] U. Hohenester, A. Trügler, P. E. Batson, and M. J. Lagos, Physical Review B **97**, 165418 (2018).

[14] B. D. Forbes and L. J. Allen, Physical Review B **94**, 014110 (2016).

[15] G. Radtke, D. Taverna, M. Lazzeri, and E. Balan, Physics Review Letters **119**, 027402 (2017).

[16] A. Govyadinov, A. A. Konečná, A. Chuvilin, S. Vélez, I. Dolado, A. Y. Nikitin, S. Lopatin, F. Casanova, L. E. Hueso, J. Aizpurua, and R. Hillenbrand, Nature Communications **8**, 95 (2017).

[17] F. S. Hage, R. J. Nicholls, J. R. Yates, D. MuCulloch, T. C. Lovejoy, N. Delby, O. L. Krivanek, K. Refson, and Q. M. Ramasse, Science Advances **4**, eaar7495 (2018).

[18] K. Sturm, Z. Naturforsch. **48a**, 233 (1993).

[19] S. K. Sinha, J. Phy.: Condens. Matter **13**, 7511 (2001).

[20] E. Burkel, J. Phys.: Condens. Matter **13**, 7627 (2001).

[21] F. S. Hage, Q. M. Ramasse, D. M. Kepaptsoglou, Ø. Prytz, A. E. Gunnaes, G. Helgesen, and R. Brydson, Physical Review B **88**, 155408 (2013).

[22] S. J. Clark, M. D. Segall, C. J. Pickard, P. J. Hasnip, M. J. Probert, K. Refson, and M. Payne, Z. Kristall. **220**, 567 (2005).

[23] K. Refson, P. R. Tulip, and S. J. Clark, Phys. Rev. B **73**, 155114 (2006).

[24] J. Serrano, A. Bosak, R. Arenal, M. Krisch, K. Watanabe, T. Taniguchi, H. Kanda, A. Rubio, and L. Wirtz, Physical Review Letters **98**, 09550 (2007).

[25] E. Rokuta, Y. Hasegawa, K. Suzuki, Y. Gamou, C. Oshima, and A. Nagashima, Physical Review Letters **79**, 4609 (1997).

[26] K. H. Michel and B. Verberck, Physical Review B **83**, 115328 (2011).